scientific reports

Check for updates

OPEN

Exploring the impact of temperature and oxygen partial pressure on the spent nuclear fuel oxidation during its dry management

A. Milena-Pérez, L. J. Bonales✉, N. Rodríguez-Villagra & H. Galán

The management of Spent Nuclear Fuel (SNF) comprises different stages in which security is demonstrated. Nevertheless, fundamental research can lead to other design options that must be considered. Currently, one of the focuses is the dry interim storage option, as the shortest-term solution until final repositories are available. During this stage, one concern is the oxidation of the fuel. If UO_2 (SNF matrix) is exposed to air at high-enough temperature, formation of U_3O_8 takes place. The larger volume of this phase could entail stresses on the SNF clad, which is the first barrier to prevent radioactive material release. It is known that this oxidation is a temperature-dependent reaction and ensuring an inert atmosphere discards any effect during SNF dry management. However, at what extent temperature and oxygen concentration would have an impact on the U_3O_8 formation is not established, being the available experimental data very scarce. We follow this oxidation in representative ranges of temperature and oxygen concentration of dry storage facilities by using in-situ Raman spectroscopy. The results show that temperature is a more-affecting factor than the oxygen concentration at the studied conditions. Therefore, efforts to limit temperatures would yield more benefits in preserving fuel matrix integrity.

There is an international and increased concern on the Spent Nuclear Fuel (SNF) integrity during SNF management for pre-disposal activities, being the interim dry storage the intermediate step before the final disposal. At present, dry storage is one of the shortest-term solutions for SNF accumulation difficulties in the near future because of the limited space in water-pool, used as a passive heat-removal system for cooling, and the uncertainty of the deep disposal operation schedule, which is the last stage planned. In dry storage conditions, the safety of the fuel must be ensured mainly in front of oxidation, which can occur at high-enough temperature in presence of oxygen, and may possibly lead to a potential mechanism affecting the clad integrity driven by the formation of U_3O_8.

Therefore, the formation of U_3O_8 and other intermediate oxides from the oxidation of UO_2, the main constituent of most of the nuclear fuels (thus being often called "Spent Nuclear Fuel matrix"), has received considerable attention through the past decades[1–7]. The study of the different parameters that can affect this reaction, such as temperature and oxygen partial pressure, is of interest for irradiated fuel under operational and accidental scenarios during handling and transport. This has been the origin of regulation limiting the exposure of fuel matrix to temperature and oxidant species[8–12].

The oxidation of UO_2 is a well-understood process, which involves a number of intermediate oxides with different characteristics. In the case of unirradiated fuel, these oxides include the generally labelled UO_{2+x}, where cubic lattice from the original UO_2 is still maintained; U_3O_7, that implies a change in the structure, obtaining a phase with a tetragonal lattice; and U_3O_8, in which lattice changes are again observed, obtaining an orthorhombic oxide. This phase is the final product of the oxidation at the range of temperatures and pressures expected during the fuel storage[4,5]. Compared to UO_2, U_3O_8 entails an increase in volume of around 36%, and comes along with spallation and pulverization of the initial UO_2 sample[5]. Therefore, the formation of U_3O_8 could lead, depending

High-Level Waste Unit, Centro de Investigaciones Energéticas, Medioambientales y Tecnológicas (CIEMAT), Avda. Complutense 40, 28040 Madrid, Spain. ✉email: Laura.bonales@ciemat.es

on the condition of a pre-existent failure in the clad, to failure propagation, splitting the clad and even allowing certain release of radioactive material[13–16].

Due to its practical importance from the nuclear safety point of view, the boundary conditions in current nuclear storage facilities at which U_3O_8 does not form are widely studied (i.e. low temperature and lack of oxygen). Other conditions impacting on the formation of U_3O_8 have been studied under the circumstances expected during dry storage of the fuel, especially focused on temperature. At the interim storage facilities, the upper limit temperature allowed in inert atmosphere for LWR fuel is 400 °C[9,11,17], to protect the fuel rod cladding[18]. During normal conditions of storage, there will be a range of temperatures lower than the maximum allowable of 400 °C. That's why most of the studies regarding the formation of U_3O_8 during oxidation of SNF have been conducted at this temperature or below[5,15,19–22]. The huge majority of these experiments have been carried out by using thermogravimetric analysis and flowing air as the oxidant phase.

About the reaction atmosphere, the fuel has been mainly studied after being exposed to air. Investigating the potential oxidation of the fuel matrix at lower oxygen partial pressures, i.e., with specific loading cells being partially inert, might bring to other alternatives to air that might delay or even prevent this oxidation. However, the literature regarding the effect of lower oxygen partial pressures than air on UO_2 oxidation is scarce. With SNF, Nakamura et al.[23] oxidized prepared defective fuel rods with burnups ranging from 14 to 30.6 GWd/tU at 200-240ºC in different atmosphere (1%, 5% and 21%O_2). At 200 °C, they found a decrease of the oxidation rate with the oxygen content and a stabilization of the U_4O_9 phase[5,24]. In addition, Kolyadin et al.[25] studied the oxidation of irradiated samples (burnups between 10.07 and 19.7 GWd/tU) with very low oxygen atmospheres (0.08%, 0.48% and 1.3%O_2) at temperatures in the range of 100–300 °C. They concluded that the lower the oxygen concentration, the slower the oxidation reaction.

Unirradiated fuel has been studied only by a few authors at different temperatures and atmospheres[2,26–28]. In addition, most of the studies published up to date were conducted by using traditional techniques, mainly thermogravimetry. This technique gives information about the kinetic behavior of UO_2 oxidation under the specified conditions, as well as the different mechanisms that take place during this reaction by studying the shape of the weight gain curves[5]. This technique measures the "bulk" oxidation of the sample, giving as a result an average O/M value reached by UO_2 after the experiment. Taking into account the possible security controls at storage facilities, it could be interesting to detect the potential early apparition of U_3O_8 and follow the progress of the reaction even if the entire sample is not yet oxidized. Only Olsen et al.[28] recently studied the oxidation of purified UO_2 in a wider range of temperatures (100–400 °C) and oxygen partial pressures (0–21%O_2). They aged the samples in a furnace with controlled atmosphere at different times (2, 25 and 48 h) and characterized ex-situ the final product at each condition by XRD. Nevertheless, more studies covering a complete range of temperatures and oxygen concentrations under the same experimental conditions are needed to support and validate the singular conclusions from each study.

In this work, we study the effect of three temperatures at and below the aforementioned maximum allowable of 400 °C[9,11] (i.e. 200, 300 and 400 °C) each of one at four different atmospheres (0.1, 1, 10, and 21% O_2) on the formation of U_3O_8, which is the terminal thermodynamic state at these conditions[29], from a fresh UO_2 surrogate, whose representativeness is proved in terms of its conservatism in relation to actual spent fuel[30]. In addition, in this study the oxidation at in-situ conditions is measured from really short times (2 min) up to longer times (3 days), depending on the oxidation products obtained at every specific condition.

In this regard, Raman spectroscopy is presented in this work as a non-destructive technique able to meet this purpose. This technique provides a fingerprint to distinguish between chemically similar compounds, as it is the case of uranium oxides. Besides, it gives the possibility to perform in-situ measurements, allowing studying the materials in the real conditions at which they will be in a real storage facility. Raman spectroscopy has been previously used in the characterization of uranium oxides[31–40]. In our laboratory, several identification studies have been carried out[41–44], and some initial tests have been performed in-situ[41,45]. However, to the best of our knowledge, this is the first time that this technique is employed to study the oxidation of UO_2 at in-situ conditions, including lower oxygen partial pressures than air. Also, the measurement protocols developed here can be directly applied in the study of irradiated fuel.

Thus, the main goal of this work is to analyze in detail and clarify the impact of changing, in a broad range of conditions, both the temperature and the oxygen concentration in the atmosphere in contact with SNF on the oxidation of the spent fuel matrix.

Results

The aim of this work is to evaluate the combined effect of the decrease in the O_2 content and the temperature on formation of the oxidized phases of UO_2. The method used to study this reaction is based in the analysis of the Raman spectra obtained at in situ conditions (0.1, 1, 10 and 21% O_2 and temperatures of 200, 300 and 400 °C). These conditions are obtained by using a Linkam stage which has been slightly modified in order to house it to a Raman spectrometer (see "Methods" section).

The Raman spectra of each oxidized UO_2 phase (i.e. UO_{2+x}, U_3O_7, U_3O_8) is well known[31,32,34,35,38,46–48] and, as it was confirmed in our previous works[41–45], this spectroscopy can unequivocally identify each phase at room temperature. At higher temperatures, we already demonstrated that the main features of the spectra corresponding to UO_2[42] and UO_{2+x}[45] do not suffer any drastic change, but as expected, all Raman bands downshift in wavenumber and increases its bandwidth with increasing temperature. Raman spectra of U_3O_7 and U_3O_8 at higher temperatures are evaluated here.

The analysis was carried out as follows: we first establish the criteria to identify the different phases i.e. determine the Raman fingerprint or Raman signature of each phase. After verifying that the characteristics corresponding to the U_3O_7 and U_3O_8 phases are not modified due to temperature, these Raman signatures are used

to analyze the spectra acquired in situ in the different experiments, i.e. the Raman spectra acquired at each time (up to 3000 s, i.e. around 2 days), temperature and O_2 concentration.

UO_2, UO_{2+x} U_3O_7 and U_3O_8 Raman signatures. The characteristic UO_2 spectrum shows (see Fig. 1A) the triply degenerate T_{2g} mode at 445 cm^{-1} (a), the LO mode at about 570 cm^{-1} (b), and the first overtone of the L-O mode (2LO) centered about 1140 cm^{-1}[31] (c). Figure 1B shows the spectrum corresponding to UO_{2+x} with x = 0.1. This x value represents the average composition of the sample, probably formed by a mixture of UO_2 and U_3O_7 in the conditions studied here[29]. As is clearly shown in the figure, with the increase in the oxidation the spectrum suffers a broadening and upshifting of the 445 cm^{-1} band (a), an increase in the intensity of the 570 cm^{-1} (b) and a decrease in the intensity of the 2LO band (c) compared with the initial UO_2 (x = 0). Moreover, the spectrum shows the apparition of a new band near 630 cm^{-1} associated to the oxidation[31,41]. It should be noted that these two bands (570 cm^{-1} and 630 cm^{-1} bands) overlap, giving a broad band centered above 600 cm^{-1}, which will be referred in this work as defects band (b)[41].

The characteristic Raman spectrum of the next oxidized phase U_3O_7 is presented in Fig. 1C. It is identified by the two bands corresponding to the T_{2g} mode (a), the band associated to the defects above 600 cm^{-1} (b) and the fading of the 2LO band originally at ~ 1140 cm^{-1}[31,41,49]. In this phase, an extra Raman feature located at about 120 cm^{-1} (c) becomes visible, which has been assigned to tetragonal distortions of the cubic lattice of UO_2, therefore confirming that the spectrum corresponds to U_3O_7[31,50].

Finally, the Raman spectrum of U_3O_8 is presented in Fig. 1D. Compared to previous oxidized phases, it is characterized by a completely different pattern. The main Raman feature is the broad triplet in the 300–500 cm^{-1} region (a), associated with the different modes of the U–O stretching in the orthorhombic lattice[46,47]. This mode has been used as a fingerprint for identification of this compound[33]. The Raman spectrum of U_3O_8 also presents a quartet of modes between 90 and 150 cm^{-1} (b), an intense peak at 240 cm^{-1} (c), and a broad band around

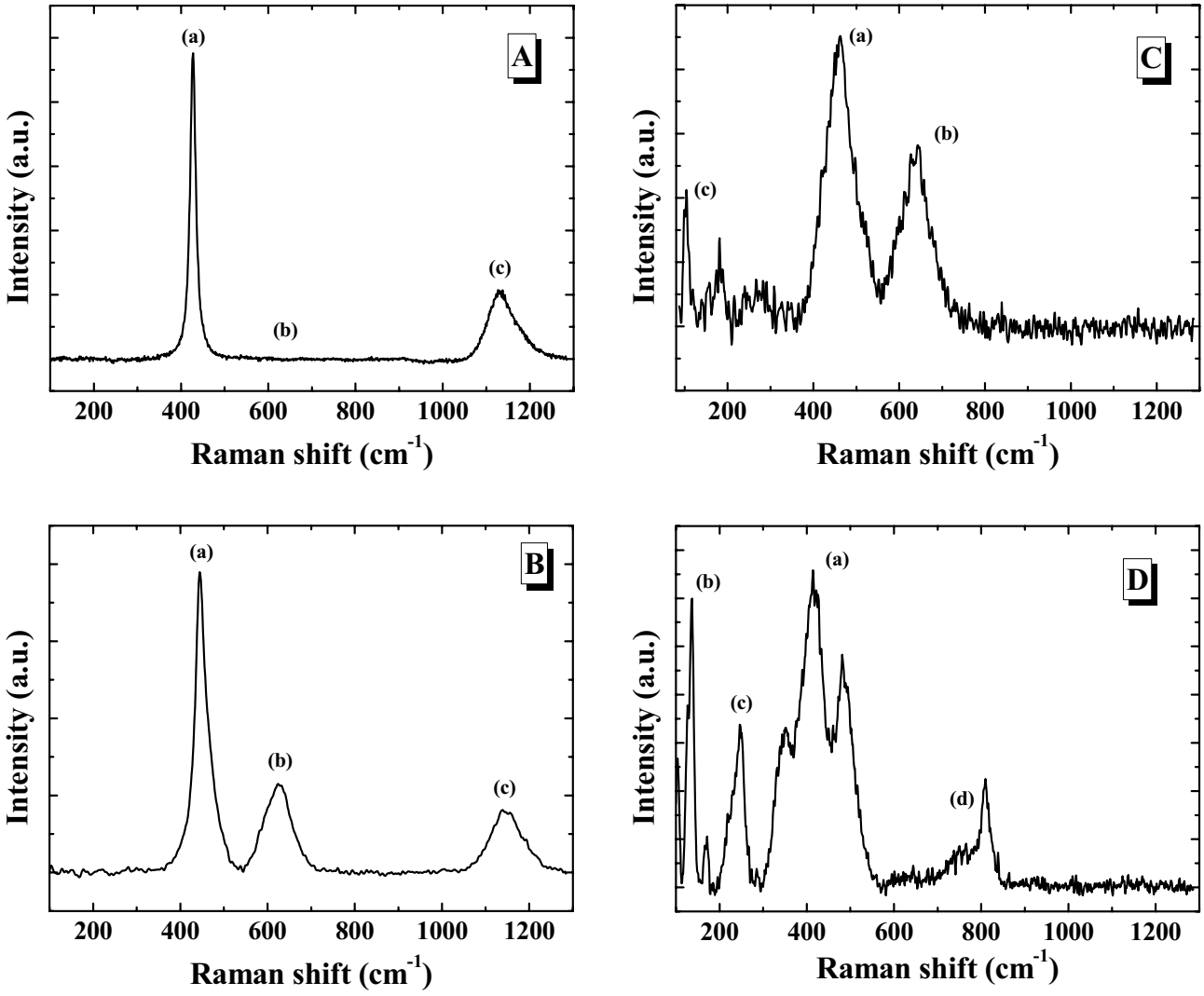

Figure 1. Raman signatures of the different uranium oxides characterized in this work, being (**A**) UO_2 (**B**) UO_{2+x} ($UO_{2.10}$) (**C**), U_3O_7 and (**D**) U_3O_8.

750 cm^{-1} together with a narrower peak at around 810 cm^{-1} (d). The assignment of these bands is more or less known, although some details are still missing[33,47,51].

As seen in Fig. 1, the evolution of the Raman spectra with the oxidation can be described as follows: the initial UO_2 spectrum varies by increasing the intensity of the band located above 600 cm^{-1} and decreasing the intensity of the band at 1140 cm^{-1} (2LO band) when oxidized to UO_{2+x}. Thereafter, when U_3O_7 is formed, the 2LO band disappears and therefore the spectrum has two intense features at 445 cm^{-1} and above 600 cm^{-1}. The change that occurs when the oxidation proceeds up to U_3O_8 is evidenced by the triplet of bands in the 300–500 cm^{-1} region.

Once we have stabilized the Raman signature of each phase, let us to check that the effect of the temperature do not modify the Raman fingerprint of the U_3O_7 and U_3O_8 phases described above. In order to reach this goal, we have measured the U_3O_7 as U_3O_8 phases as a function of temperature at inert conditions (Ar) (Fig. 2A,B). According to the results, the main Raman modes suffer a slight broadening and shift to lower wavenumbers. Nevertheless, the main spectral features remain constant for the working temperatures, allowing us using them to identify the different oxides not only at room temperature but also at high temperature up to 400 °C. On the one hand, for U_3O_7 (Fig. 2A), the disappearance of the 2LO band with respect to the UO_{2+x} spectrum is used. On the other hand, for U_3O_8 (Fig. 2B), the presence of the broad signal in the 300–500 cm^{-1} region, although the triplet is not as evident as at room temperature, can still be used for a quick identification of this phase.

In situ Raman study of the UO_2 oxidation at different atmospheres and temperatures. By using the Raman signatures described above we have identified the formation of each phase formed at each time (up to 3000 s, i.e. around 2 days) at the testing conditions (0.1, 1, 10 and 21% O_2 and temperatures of 200, 300 and 400 °C). Next paragraphs show some representative results obtained at different conditions studied in this work. They have been selected in order to present an illustrative picture of the possible scenarios that could be

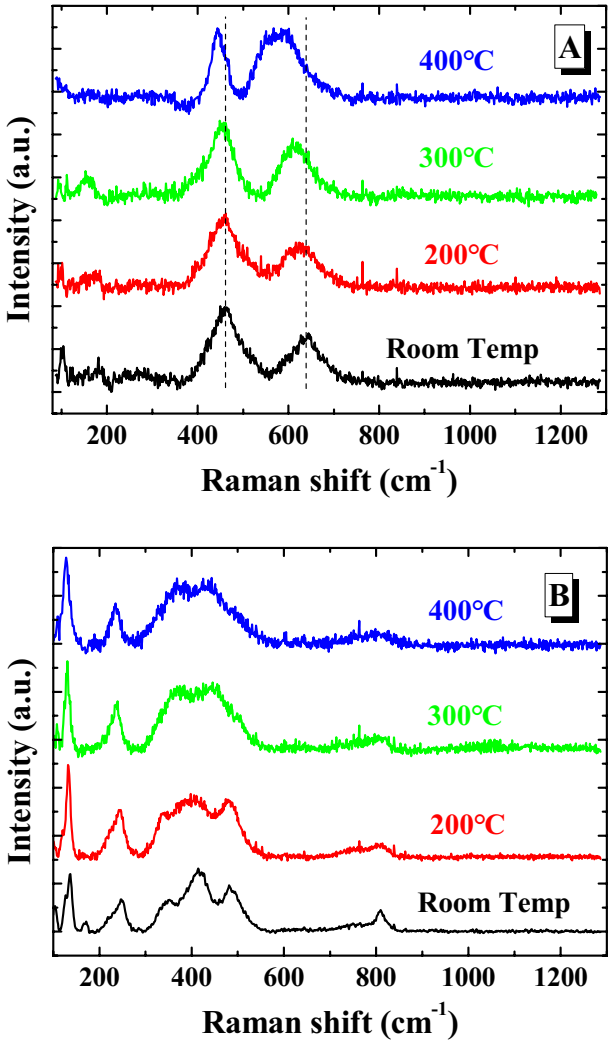

Figure 2. Raman spectra of (**A**) U_3O_7 and (**B**) U_3O_8 under inert conditions (Ar) as a function of temperature in the region studied in this work.

considered in new design options of dry storage facilities. The rest of the results, covering the complete range of experiments, can be found at the supplementary information.

Figure 3 shows the spectra as a function of time obtained at the lowest temperature and O_2 concentration studied (200 °C and 0.1%). In the Figure, the typical features of the hyperstoichiometric UO_{2+x} phase are obtained in the whole time period experimented i.e. three main bands at around 445, above 600 and 1140 cm^{-1} corresponding to the aforementioned T_{2g}, "defects band" and 2LO modes. It should be noted that the evolution of the spectra as a function of the oxidation time is demonstrated by the continuous increase in the intensity of the band above 600 cm^{-1} and the decrease in the intensity of the 2LO band.

At same O_2 concentration (0.1%) and higher temperature (300 °C) the spectra show the formation of UO_{2+x} up to 18 min (Fig. 4A), note the three bands at around 445, 600 and 1140 cm^{-1}. At times close to 24 min the disappearance of the 2LO band (1140 cm^{-1}) becomes evident, indicating the formation of U_3O_7 (Fig. 4B). This phase prevails up to times of 21 h, after this (at times ranging from 22 to 45 h) the apparition of the trident evidences the formation of U_3O_8 (Fig. 4C).

Same three phases (UO_{2+x}, U_3O_7 and U_3O_8) have been detected at 21% O_2 and 300 °C (Fig. 5). At short times (up to 23 min) the spectra have the three main bands corresponding to the UO_{2+x} phase, then the disappearance of the 2LO band (1140 cm^{-1}) evidence the formation of U_3O_7 (Fig. 5A), and finally from around 5 h the spectra correspond to the U_3O_8 phase (Fig. 5B).

From the spectra acquired at the different experimental conditions, and previously presented, valuable information can be extracted. The spectral differences aforementioned have been associated to the structural changes that occur in UO_2 when starts to oxidize first to UO_{2+x}, maintaining the cubic lattice; then proceeding via U_3O_7 with such a distortion that the lattice goes to a tetragonal intermediate; and finally oxidizing up to U_3O_8, which is orthorhombic and present completely different Raman bands.

Discussion

The spectra acquired at the different experimental conditions, and previously presented, have been interpreted in terms of the oxidation degree of UO_2. The O/U ratio has been estimated according to the evolution of the Raman spectra with time. This assessment has allowed us characterizing the overall reaction and to divide it into three different phases UO_{2+x}, U_3O_7 and U_3O_8. First of all, the initial step of the reaction has been evaluated by determination of "x" in the structure UO_{2+x}, to confirm the increasing oxygen incorporation to the lattice with time, but not observing a substantial structural change reflected in the spectra. With this purpose, we have used a previous analysis of the Raman spectra as a function of x[41], taking also into account the temperature correction factor[45], as shown in Eqs. (1) and (2).

$$\Delta v_{630}\left(cm^{-1}\right) = -(610 \pm 60)x - (0.049 \pm 0.003)T(K), (I_{630}/I_{445} < 0.24), \quad (1)$$

$$\Delta v_{630}\left(cm^{-1}\right) = -(90 \pm 20)x - (0.049 \pm 0.003)T(K), (0.27 < I_{630}/I_{445} < 0.24). \quad (2)$$

In Eqs. (1) and (2), Δv_{630} is defined as $\Delta v_{630} = v_{630} - v_{int}$, being v_{630} the Raman shift of the band associated to the increase in the oxidation degree[31,35,41,51–53], and v_{int} the Raman shift of the linear fit intercept. To obtain both Raman shifts, a detailed profile analysis has been carried out in every single spectrum. Central position of the spectral bands was obtained by the second derivative method[54]. The use of two equations to calculate x responds to the distinct regions observed in this transition, as reported by Elorrieta et al.[41].

Secondly, a second step in the oxidation reaction is defined, where the intermediate U_3O_7 phase is mainly obtained and interpreted as a stabilization phase of the reaction before reaching the final oxidation product. This phase has been associated with an O/U between 2.25 and 2.40, according to different values reported in literature[7,31,55,56]. The Raman spectrum of this phase shows two strong bands (the T_{2g} mode at ~ 445 cm^{-1} and the

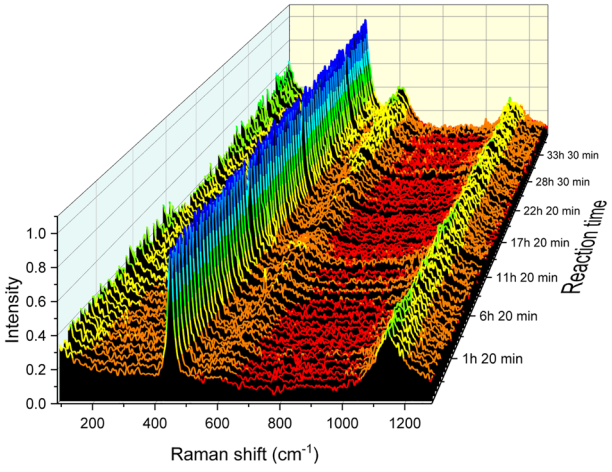

Figure 3. Raman spectra acquired during the experiment at 200 °C and 0.1%O_2.

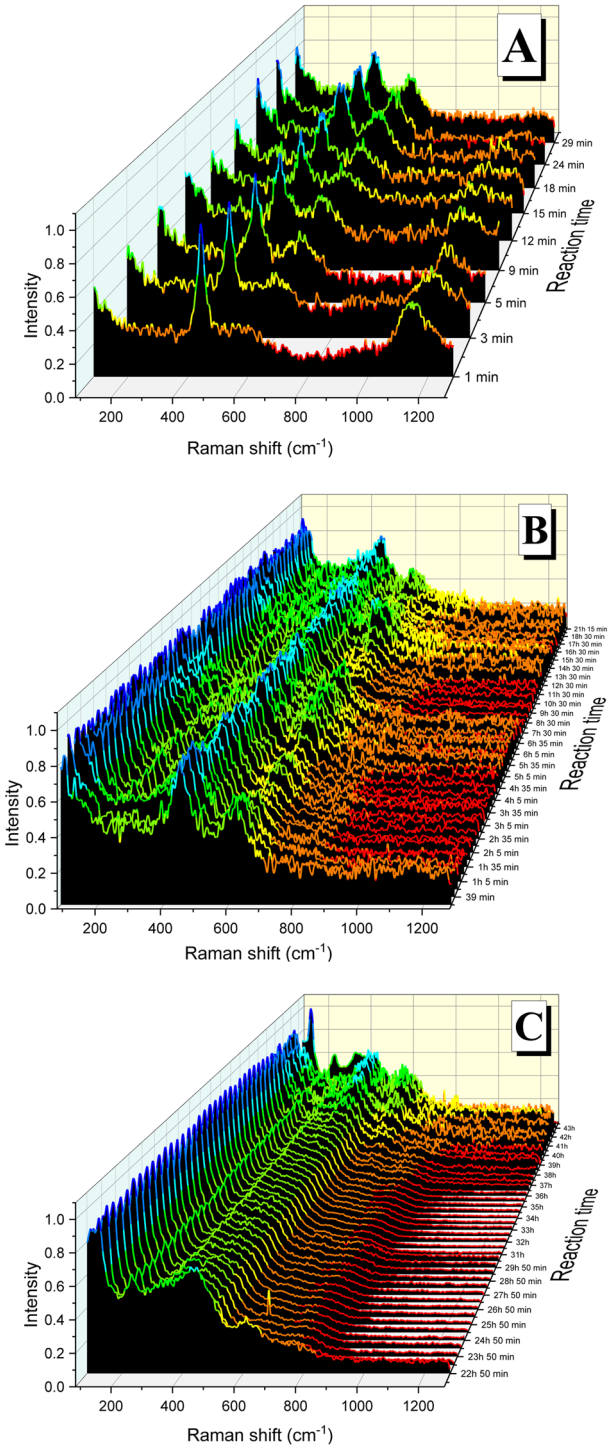

Figure 4. Raman spectra acquired during the experiment at 300 °C and 0.1%O_2 showing the formation of different oxidized phases from the initial UO_2: (**A**) UO_{2+x} up to 18 min, (**B**) U_3O_7 from 24 min to 21 h and (**C**) U_3O_8 from 22 h to the end of the experiment.

oxygen-clusters-related ~ above 600 cm^{-1} band), and the lack of the 2LO mode, which makes it distinct from the UO_2 and the UO_{2+x} spectrum[31,38,41,57]. Finally, a third step in the reaction is defined by the presence of acquired spectra corresponding to the U_3O_8 phase, which is associated with the final of the oxidation process (O/U = 2.67).

By following these guidelines, the overall progress of the oxidation in the different conditions studied is presented in Fig. 6, in terms of the O/U ratio vs reaction time. The results have been plotted distinguishing temperatures (200, 300 and 400 °C) and oxygen partial pressures at which the oxidation has been carried out (0.1%, 1%, 10% and 21%O_2).

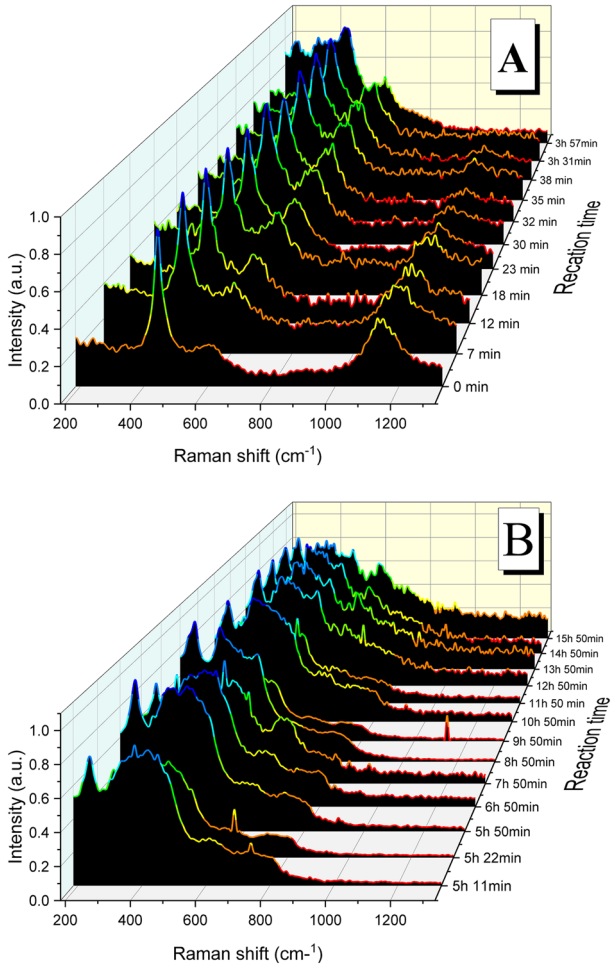

Figure 5. Raman spectra acquired during the experiment at 300 °C and 21%O_2 showing the formation of different oxidized phases: (**A**) UO_{2+x} and U_3O_7 during the first 5 h and (**B**) U_3O_8 from 5 h on.

At 200 °C, only the UO_{2+x} phase is observed, regardless of the oxygen concentration, in the whole duration of the experiments (approximately 2 days per temperature and oxygen concentration). The effect of the limited availability of oxygen in this low temperature is the extent of the UO_{2+x} phase, i.e. the O/U value. From Eqs. (1) and (2), we have calculated the O/U, obtaining that with 0.1%O_2 is O/U = 2.07 ± 0.03. This value grows with oxygen concentration, resulting in O/U = 2.17 ± 0.05 with 1%O_2; O/U = 2.18 ± 0.05 with 10%O_2; and O/U = 2.24 ± 0.06 with air (21%O_2) (Fig. 6A–D, respectively). Thus, no formation of higher oxides has been detected in any case. In addition, it should be highlighted that the effect of a higher presence of the oxidant is to accelerate the first step of the reaction with time. This effect has been previously reported as a consequence of the diffusion mechanism in the first part of the oxidation of UO_2[1,4,7,58]. In fact, Blackburn et al.[2] measured the oxidation of unirradiated UO_2 at 200 °C covering a range of oxygen concentrations from 0.07 to 100%O_2. They reported a lack of effect on the oxidation degree between 20 and 100%O_2, but stated that a decrease of the oxidation occurred in the 0.07–20%O_2 range when the oxygen concentration was low, being consistent with the results of this work.

On the other hand, at 400 °C the U_3O_8 phase is prevalent, independently of the oxygen concentration. In the most extreme case, i.e. 21%O_2, only U_3O_8 is observed even at the very beginning of the experiment, giving an idea of the quickness of the oxidation at these conditions. These data could be taken into account in new designs for nuclear fuel storage facilities given the risk of fuel exposure to air at this temperature. With lower oxygen partial pressures, it is possible to observe the lesser oxidized phases UO_{2+x} and U_3O_7. However, the temporal frame of the reaction is very short, being U_3O_8 the only oxide observed from 20 min even with the lowest oxygen concentration, 0.1%. Earlier in this case, UO_{2+x} spectra, with the x value continuously increasing, are acquired during approximately 10 min. At this point, the transformation to U_3O_7 seems to happen, obtaining a couple of spectra corresponding to this phase during the period 10–20 min (Fig. 6A). The increase of the oxygen presence results in a shortening of the time where the lower oxides are observed, obtaining U_3O_8 spectra from around 15 min with 1%O_2 and from around 10 min with 10%O_2 (Fig. 6B,C, respectively).

This tendency, maintained through all the oxygen concentrations studied, emphasizes the importance of the fuel temperature, and points out to put efforts on limit the fuel temperature rather than partially inertize (above 0.1%O_2), which would yield more benefits in preserving fuel matrix integrity. These results, agreeing with

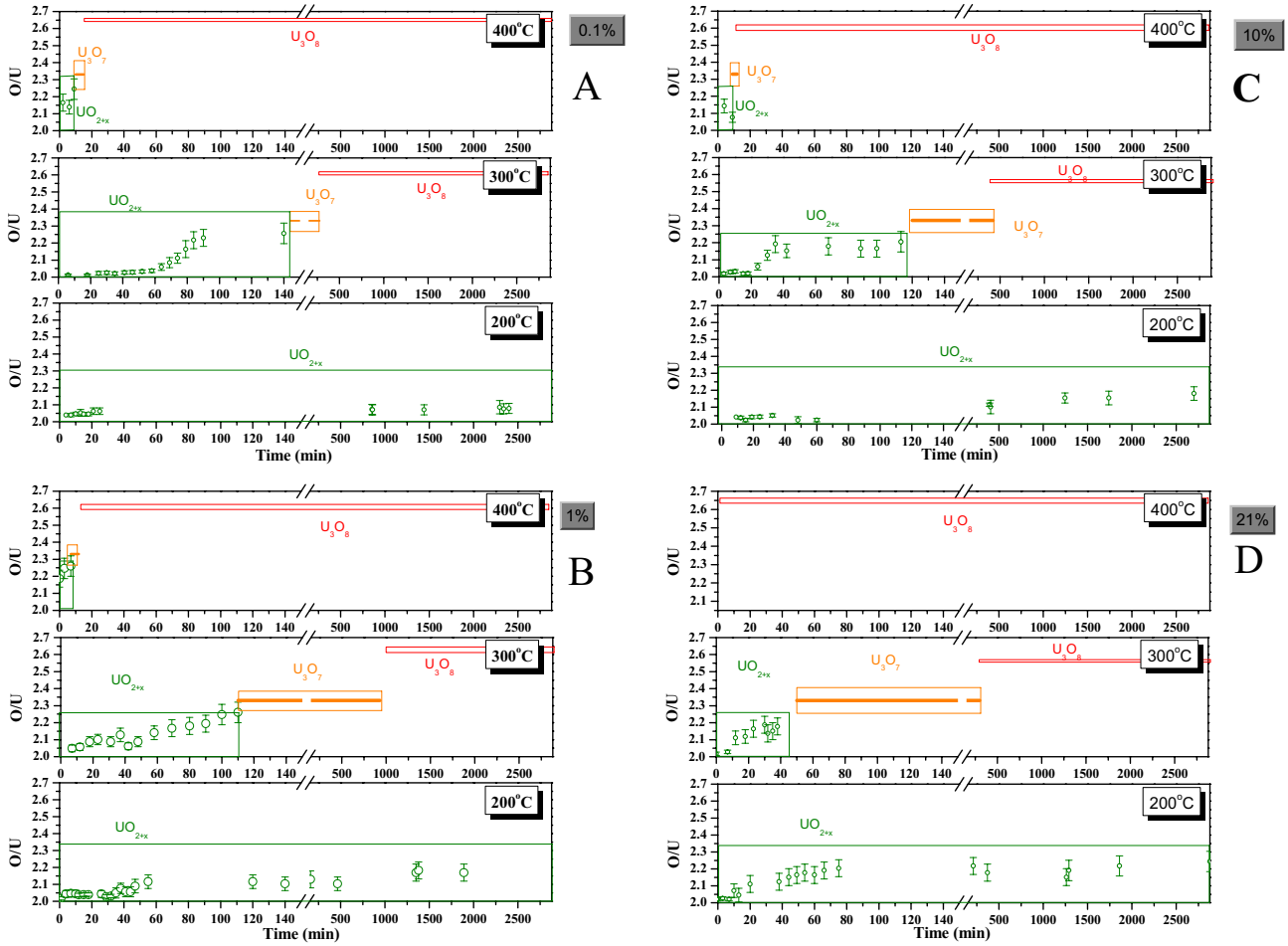

Figure 6. O/U ratio vs reaction time in the different temperatures and oxygen partial pressures studied.

published studies using other techniques, such as those reported by Olsen et al.[28], who by using XRD observed the formation of a 100% of U_3O_8 at 400 °C within 2 h when any oxygen is present (the lack of a measurement at shorter times in the referenced study makes a deep comparison of the early apparition of U_3O_8 impossible). This behavior is comparable to the oxidation of irradiated fuel, as demonstrated in the study by Hastings et al.[22]. They studied the oxidation of CANDU fragments irradiated at low burnup levels (8 GWd/tU) in air, in the same temperature range than this work (200–400 °C). At 200 °C, they did not observe any weight change during 24 h of experiments. However, at 400 °C, they reported a severe sheath splitting due to the formation of U_3O_8 in less than 24 h.

At intermediate temperatures, i.e. 300 °C, the formation of U_3O_8 is not as fast as in the previous case, but this phase is still clearly observed from a time around 24 h in all the cases. At 300 °C, the effect of decreasing the oxygen concentration is to delay the formation of U_3O_8, extending the temporal frame when UO_{2+x} and U_3O_7 are present. Thus, at the lowest oxygen concentration, 0.1%O_2, UO_{2+x} spectra are acquired during the first 140 min approximately, with increasing x. From that moment, U_3O_7 becomes visible and appears until around 10 h of experiment, when U_3O_8 becomes principal. When increasing the oxygen partial pressure, the observed results indicate that the time range where UO_{2+x} is observed is increasingly shorter, and U_3O_7 phase appears earlier. However, the final result of every experiment at this temperature is the formation of U_3O_8 at a time around 16 h for the lowest oxygen concentrations, and even earlier when the amount of oxygen present is higher. This would suggest that the temperature dependence over oxygen content on the oxidation of UO_2 is therefore more evident at relatively high temperature, especially from 300 °C. In fact, it seems that once that a certain threshold temperature for the formation of U_3O_8 is exceeded, this phase will be formed even with low oxygen availability (as low as 0.1%). Therefore, the effect of this oxygen decrease will be to delay the presence of U_3O_8.

From the analysis of Fig. 6D, one may note that the observed change in the O/U ratio resembles the typical sigmoidal behavior characteristic of the oxidation. In a similar time scale, this pattern has been found in thermogravimetric analysis of UO_2 oxidation[7]. This fact reinforces the use of Raman as a suitable technique for studying this reaction, and validates the conclusions obtained here.

Conclusions

In this work, representative oxidation experiments with the aim to determine the combined effect of partial inertization and temperature on the formation of U_3O_8 are performed in order to be considered in new design options of fuel storage facilities. Specifically, we study the impact of the oxygen partial pressure (0.1 to 21%O_2) and temperature (200–400 °C) in the oxidation of fresh UO_2 (labelled as P3 in the reference[30]). With this purpose, Raman spectroscopy has been selected as a suitable technique, given first its capacity to analyze the oxidized compounds of UO_2, second its application at in-situ conditions to follow the formation of the oxidation products in a very long time frame (from min up to days), and third this protocol could be implemented in the analysis of irradiated nuclear fuel.

At 200 °C, no quantitative oxidation of UO_2 to higher oxides has been detected, neither U_3O_7 nor U_3O_8, at any of the different atmospheres studied. Given the conservativeness of fresh fuel compared to irradiated fuel, this temperature ensures a low oxidation of SNF matrix that can be considered as a "first barrier" for the spent fuel dry management activities, regardless of the content of oxygen at which the fuel may be exposed.

On the other hand, at 400 °C the oxidation of UO_2 is extremely fast whatever the oxygen concentration may be. In fact, although the lower oxygen slows down the reaction, even at oxygen concentrations as low as 0.1%, the formation of U_3O_8 occurs within 2 h. The larger volume of this phase could entail stresses on the SNF clad, which is the second barrier to prevent radioactive material release.

At intermediate temperatures, i.e. 300 °C, the decrease of the formation of U_3O_8 is clearly observed, confirming the predominant effect of the temperature over the oxygen concentration at which UO_2 is exposed. However, U_3O_8 is detected within 24 h for all oxygen concentrations studied.

All in all, the results of this work indicate that temperature is the main factor of the oxidation of fuel while the oxygen concentration of the atmosphere, up to 0.1%O_2, only affects the reaction rate without preventing it to occur. As a consequence of the present work it could be noticed that, in order to avoid the oxidation of the fuel matrix to U_3O_8, keeping the fuel at low temperatures could be very effective. On the other hand, the control of the oxygen-content (above 0.1%O_2) in the atmosphere where the UO_2 is exposed is less effective.

Finally, in order to extrapolate these conclusions to other conditions, further research not only studying other intermediate temperatures, but also other characteristics of the starting materials and involving other characterization techniques will be carried out.

Methods

The fuel analogues studied consisted of powdered UO_2 samples coming from monoliths of unirradiated sintered UO_2 pellets that were crushed into powder in a Mixer Mill MM 400 (Retsch). The resulting powder was used with no further sieving treatment, giving place to a material with a wide particle size distribution (average particle size 5.64 ± 0.07 µm, but with particle's sizes ranging from ~ 1 µm up to ~ 10 µm). Specific surface area of the material was measured by applying the BET method (with N_2) and was found to be 0.18 ± 0.01 m^2 g^{-1}. Initial O/U of the substrate is 2.002 ± 0.001. This material has been characterized in detail in our laboratory (labelled as P3 in Ref.[30]).

The gases used in this study with different oxygen concentration were supplied by Air Liquide (France). These gases comprised a mixture of oxygen and nitrogen in different proportions, giving place to three special mixtures as follows: 0.1%O_2–99.9%N_2; 1%O_2–99%N_2; 10%O_2–90%N_2. Finally, synthetic air was also provided by Air Liquide, with a licensed composition of 20 ± 1%O_2, being the rest N_2. An extra gas line of Ar is used when inert conditions are required. A certified purity higher than 99.999% is applied for all the gases.

Raman spectra were acquired by means of a Horiba LabRam HR Evolution spectrometer (Jobin Yvon Technology). A red He–Ne laser beam ($\lambda = 632.8$ nm) was focused onto the sample through the 50 × objective of an Olympus BX41 microscope. The scattered radiation was then collected with the same objective, dispersed with a 600 grooves/mm grating, and finally detected with a Peltier-cooled CCD detector (256 × 1024 pixels). For the in-situ measurements, the sample was placed inside a Linkam THMS600 temperature-controlled pressure stage. This stage allows maintaining the sample in a closed environment and focusing the incident radiation through a central overture in order to acquire the spectra. The sample temperature is controlled by using a T95-Linkpad temperature controller, which provides temperature stability better than 0.2 °C. Atmospheric environment can be selected changing the gas tubes in a quick-fit.

The experimental work has consisted, first, of placing the sample inside the Linkam stage and closing the lid assembly. After overnight inertization of the chamber with a low flow of Ar gas in order to remove the oxygen, the sample is heated at 10 °C min^{-1} up to the experimental temperature (i.e. 200, 300 or 400 °C), still with the Ar atmosphere to prevent undesirable oxidation. Once the chosen temperature is reached, it is maintained during 30 min to allow thermal stabilization of the sample. After that, the gas is switched to the specific oxidant gas, depending on the experiment (i.e. 0.1, 1, 10 or 21%O_2). Raman spectra are acquired continuously at random locations of the sample surface within typically 50 s of acquisition and 2 accumulations in the 100–1300 cm^{-1} range. These acquisition conditions have been confirmed as low enough to not oxidize the samples by local heating[41].

Data availability

The datasets generated during and/or analyzed during the current study are available from the corresponding author on reasonable request.

Received: 21 December 2022; Accepted: 1 February 2023
Published online: 03 February 2023

References

1. Aronson, S., Roof, R. & Belle, J. Kinetic study of the oxidation of uranium dioxide. *J. Chem. Phys.* **27**, 137–144. https://doi.org/10.1063/1.1743653 (1957).
2. Blackburn, P. E., Weissbart, J. & Gulbransen, E. A. Oxidation of uranium dioxide. *J. Phys. Chem.* **62**, 902–908. https://doi.org/10.1021/j150566a002 (1958).
3. Hoekstra, H. R., Santoro, A. & Siegel, S. The low temperature oxidation of UO2 and U4O9. *J. Inorg. Nucl. Chem.* **18**, 166–178. https://doi.org/10.1016/0022-1902(61)80384-9 (1961).
4. Ohashi, H., Noda, E. & Morozumi, T. Oxidation of uranium dioxide. *J. Nucl. Sci. Technol.* **11**, 445–451. https://doi.org/10.1080/18811248.1974.9730692 (1974).
5. McEachern, R. J. & Taylor, P. A review of the oxidation of uranium dioxide at temperatures below 400°C. *J. Nucl. Mater.* **254**, 87–121. https://doi.org/10.1016/S0022-3115(97)00343-7 (1998).
6. Rousseau, G. *et al.* A detailed study of UO2 to U3O8 oxidation phases and the associated rate-limiting steps. *J. Nucl. Mater.* **355**, 10–20. https://doi.org/10.1016/j.jnucmat.2006.03.015 (2006).
7. Quémard, L. *et al.* On the origin of the sigmoid shape in the UO2 oxidation weight gain curves. *J. Eur. Ceram. Soc.* **29**, 2791–2798. https://doi.org/10.1016/j.jeurceramsoc.2009.04.010 (2009).
8. IAEA. *Storage of Spent Nuclear Fuel. Report No. Safety Standards Series No. SSG-15* (International Atomic Energy AgencyVienna, 2012).
9. U.S.NRC. *Spent Fuel Project Office Interim Staff Guidance—22: Potential Rod Splitting Due to Exposure to an Oxidizing Atmosphere During Short-Term Cask Loading operatIons in LWR or Other Uranium Oxide Based Fuel* (Nuclear Regulatory Commission, 2006).
10. U.S.NRC. *Standard Review Plan for Spent Fuel Dry Storage Systems and Facilities* (Nuclear Regulatory Commission, 2017).
11. U.S.NRC. *Spent Fuel Project Interim Staff Guidance—11: Cladding Considerations for the Transportation and Storage of Spent Fuel* (Nuclear Regulatory Commission, 2003).
12. U.S.NRC. *Standard Review Plan for Spent Fuel Transportation* (Nuclear Regulatory Commission, 2019).
13. Novak, J., Hastings, I. J., Mizzan, E. & Chenier, R. J. Post irradiation behavior of UO2 fuel I: Elements at 220 to 250°C in air. *Nucl. Technol.* **63**, 254–265 (1983).
14. Boase, D. G. & Vandergraaf, T. T. The Canadian spent fuel storage canister: Some materials aspects. *Nucl. Technol.* **32**, 60–71. https://doi.org/10.13182/NT77-A31738 (1977).
15. Einziger, R. E. & Strain, R. V. Behavior of breached PWR spent-fuel rods in an air atmosphere between 250°C and 360°C. *Nucl. Technol.* **75**, 82–95 (1986).
16. Herranz, L. E. & Feria, F. Spent fuel rod splitting due to UO2 oxidation during dry storage: Assessment of the database. *Prog. Nucl. Energy* **51**, 201–206. https://doi.org/10.1016/j.pnucene.2008.09.006 (2009).
17. U.S.NRC. *10 CFR Part 72—Licensing Requirements for the Independent Storage of Spent Nuclear Fuel, High-Level Radioactive Waste and Reactor-Related Greater than Class C Waste* (Nuclear Regulatory Commission, 2000).
18. Richmond, D. J. & Geelhood, K. J. FRAPCON analysis of cladding performance during dry storage operations. *Nucl. Eng. Technol.* **50**, 306–312. https://doi.org/10.1016/j.net.2018.01.003 (2018).
19. Einziger, R. E. & Cook, J. A. LWR Spent Fuel Dry Storage Behavior at 229°C. (1984).
20. Thomas, L. E., Charlot, L. A., Coleman, J. E. & Knoll, R. W. *Storage of LWR (Light-Water-Reactor) Spent Fuel in Air*. (Pacific Northwest Laboratory, 1989).
21. Woodley, R. E., Einziger, R. E. & Buchanan, H. C. Measurement of the oxidation of spent fuel between 140 and 225°C. *Nucl. Technol.* **85**, 74–88. https://doi.org/10.13182/NT89-A34229 (1989).
22. Hastings, I. J., McCracken, D., Novak, J. & Nash, K. *Behaviour in Air at 175–400 Degrees C of Irradiated UO2 Fuel*. 27 (Canada, 1984).
23. Nakamura, J., Otomo, T., Kikuchi, T. & Kawasaki, S. Oxidation of fuel rod under dry storage condition. *J. Nucl. Sci. Technol.* **32**, 321–332. https://doi.org/10.1080/18811248.1995.9731712 (1995).
24. Hanson, B. *The Burnup Dependence of Light Water Reactor Spent Fuel Oxidation* (Pacific Northwest National Laboratory, 1998).
25. Kolyadin, A. B., Mishin, V. Y., Mishin, K. Y., Aloy, A. S. & Koltsova, T. I. Behavior of UO2 in the RBMK-1000 Spent Fuel under Oxidizing Conditions. *MRS Proc. 824*, CC8.51. https://doi.org/10.1557/PROC-824-CC8.51 (2011).
26. Tucker, P. In *Proceedings of a Workshop Held at Berkeley Nuclear Laboratories*. 7–9.
27. Bae, K. K., Kim, B. G., Lee, Y. W., Yang, M. S. & Park, H. S. Oxidation behavior of unirradiated UO2 pellets. *J. Nucl. Mater.* **209**, 274–279. https://doi.org/10.1016/0022-3115(94)90263-1 (1994).
28. Olsen, A. M., Schwerdt, I. J., Richards, B. & McDonald, L. W. Quantification of high temperature oxidation of U3O8 and UO2. *J. Nucl. Mater.* **508**, 574–582. https://doi.org/10.1016/j.jnucmat.2018.06.025 (2018).
29. Loopstra, B. O. The phase transition in α-U3O8 at 210°C. *J. Appl. Crystallogr.* **3**, 94–96. https://doi.org/10.1107/S0021889870005701X (1970).
30. Milena-Pérez, A., Rodríguez-Villagra, N., Fernández, S. & Nunez, A. Thermal air oxidation of UO2: Joint effect of precursor's nature and particle size distribution. *Under Rev. Progr. Nucl. Energy* (2022).
31. He, H. & Shoesmith, D. Raman spectroscopic studies of defect structures and phase transition in hyper-stoichiometric UO2+x. *Phys. Chem. Chem. Phys.* **12**, 8108–8117. https://doi.org/10.1039/b925495a (2010).
32. Desgranges, L., Baldinozzi, G., Simon, P., Guimbretiere, G. & Canizares, A. Raman spectrum of U4O9: A new interpretation of damage lines in UO2. *J. Raman Spectrosc.* **43**, 455–458. https://doi.org/10.1002/jrs.3054 (2011).
33. Miskowiec, A. *et al.* Additional complexity in the Raman spectra of U3O8. *J. Nucl. Mater.* **527**, 151790. https://doi.org/10.1016/j.jnucmat.2019.151790 (2019).
34. Livneh, T. Resonant Raman scattering in UO_2 revisited. *Phys. Rev. B* **105**, 045115. https://doi.org/10.1103/PhysRevB.105.045115 (2022).
35. Livneh, T. & Sterer, E. Effect of pressure on the resonant multiphonon Raman scattering in UO2. *Phys. Rev. B* **73**, 085118. https://doi.org/10.1103/PhysRevB.73.085118 (2006).
36. Desgranges, L., Canizares, A. & Simon, P. Annealing of the Raman defect peaks in He-implanted UO2. *J. Nucl. Mater.* **559**, 153405. https://doi.org/10.1016/j.jnucmat.2021.153405 (2022).
37. Jegou, C. *et al.* Raman micro-spectroscopy of UOX and MOX spent nuclear fuel characterization and oxidation resistance of the high burn-up structure. *J. Nucl. Mater.* **458**, 343–349. https://doi.org/10.1016/j.jnucmat.2014.12.072 (2015).
38. Manara, D. & Renker, B. Raman spectra of stoichiometric and hyperstoichiometric uranium dioxide. *J. Nucl. Mater.* **321**, 233–237. https://doi.org/10.1016/S0022-3115(03)00248-4 (2003).
39. Rondahl, S. H. *et al.* Comparing results of X-ray diffraction, μ-Raman spectroscopy and neutron diffraction when identifying chemical phases in seized nuclear material, during a comparative nuclear forensics exercise. *J. Radioanal. Nucl. Chem.* **315**, 395–408. https://doi.org/10.1007/s10967-017-5666-3 (2018).
40. Milena-Pérez, A. *et al.* Raman spectroscopy coupled to principal component analysis for studying UO2 nuclear fuels with different grain sizes due to the chromia addition. *J. Nucl. Mater.* **543**, 152581. https://doi.org/10.1016/j.jnucmat.2020.152581 (2021).
41. Elorrieta, J. M., Bonales, L. J., Rodríguez-Villagra, N., Baonza, V. G. & Cobos, J. A detailed Raman and X-ray study of UO2+x oxides and related structure transitions. *Phys. Chem. Chem. Phys.* **18**, 28209–28216. https://doi.org/10.1039/C6CP03800J (2016).

42. Elorrieta, J. M., Bonales, L. J., Baonza, V. G. & Cobos, J. Temperature dependence of the Raman spectrum of UO2. *J. Nucl. Mater.* **503**, 191–194. https://doi.org/10.1016/j.jnucmat.2018.03.015 (2018).
43. Elorrieta, J. M. *et al.* Laser-induced oxidation of UO2: A Raman study. *J. Raman Spectrosc.* **49**, 878–884. https://doi.org/10.1002/jrs.5347 (2018).
44. Bonales, L. J., Elorrieta, J. M., Menor-Salván, C. & Cobos, J. The behavior of unirradiated UO2 and uraninite under repository conditions characterized by Raman. *MRS Adv.* **1**, 4157–4162. https://doi.org/10.1557/adv.2017.203 (2017).
45. Elorrieta, J. M., Bonales, J. L., Rodríguez-Villagra, N., Baonza, G. V. & Cobos, J. Spent fuel matrix oxidation studies under dry storage conditions. *MRS Adv.* **2**, 675–680. https://doi.org/10.1557/adv.2017.3 (2017).
46. Allen, G. C., Butler, I. S. & Nguyen Anh, T. Characterisation of uranium oxides by micro-Raman spectroscopy. *J. Nucl. Mater.* **144**, 17–19. https://doi.org/10.1016/0022-3115(87)90274-1 (1987).
47. Butler, I. S., Allen, G. C. & Tuan, N. A. Micro-Raman spectrum of triuranium octoxide, U3O8. *Appl. Spectrosc.* **42**, 901–902 (1988).
48. Marlow, P. G., Russell, J. P. & Hardy, J. R. Raman scattering in uranium dioxide. *Philos. Mag. J. Theor. Exp. Appl. Phys.* **14**, 409–410. https://doi.org/10.1080/14786436608219022 (1966).
49. Elorrieta, J. M., Milena-Pérez, A., Vigier, J.-F., Bonales, L. J. & Rodríguez-Villagra, N. New insights into the structural transition from UO2+x to U3O7 by quantitative Raman spectroscopy. *Phys. Chem. Chem. Phys.* **24**, 28394–28402. https://doi.org/10.1039/D2CP03573A (2022).
50. Michel, D., y Jorba, M. P. & Collongues, R. Study by Raman spectroscopy of order-disorder phenomena occurring in some binary oxides with fluorite-related structures. *J. Raman Spectrosc.* **5**, 163–180 (1976).
51. Palacios, M. L. & Taylor, S. H. Characterization of uranium oxides using in situ micro-Raman spectroscopy. *Appl. Spectrosc.* **54**, 1372–1378. https://doi.org/10.1366/0003702001951057 (2000).
52. Desgranges, L., Baldinozzi, G., Simon, P., Guimbretiere, G. & Canizares, A. Raman spectrum of U4O9: A new interpretation of damage lines in UO2. *J. Raman Spectrosc.* **43**, 455–458. https://doi.org/10.1002/jrs.3054 (2012).
53. Jégou, C. *et al.* Raman spectroscopy characterization of actinide oxides (U1−yPuy)O2: Resistance to oxidation by the laser beam and examination of defects. *J. Nucl. Mater.* **405**, 235–243. https://doi.org/10.1016/j.jnucmat.2010.08.005 (2010).
54. Talsky, G. *Derivative Spectrophotometry: Low and High Order* (VCH Publishers, 1994).
55. Leinders, G., Bes, R., Kvashnina, K. O. & Verwerft, M. Local structure in U(IV) and U(V) environments: The case of U3O7. *Inorg. Chem.* **59**, 4576–4587. https://doi.org/10.1021/acs.inorgchem.9b03702 (2020).
56. Leinders, G. *et al.* Assessment of the U3O7 crystal structure by X-ray and electron diffraction. *Inorg. Chem.* **55**, 9923–9936. https://doi.org/10.1021/acs.inorgchem.6b01941 (2016).
57. Liu, N. *et al.* Influence of Gd doping on the structure and electrochemical behavior of UO2. *Electrochim. Acta* **247**, 496–504. https://doi.org/10.1016/j.electacta.2017.07.006 (2017).
58. Poulesquen, A., Desgranges, L. & Ferry, C. An improved model to evaluate the oxidation kinetics of uranium dioxide during dry storage. *J. Nucl. Mater.* **362**, 402–410. https://doi.org/10.1016/j.jnucmat.2007.01.084 (2007).

Acknowledgements

The work presented here has been funded by ENRESA in the project: Nº 079-CO-IA-2018-0007 "Unirradiated UO_2 Oxidation Tests and associated analyses".

Author contributions

N.R.V. and L.J.B. conceived the project idea. A.M.P. performed the oxidation experiments and the Raman spectra acquisitions. L.J.B. and A.M.P. performed the data processing, interpretation, analyzed the spectra and drafting. From the beginning of the idea to data extraction, data processing, interpretation, drafting, and revising the text was supervised by N.R.V and H.G. A.M.P. wrote the initial draft and L.J.B., N.R.V. and H.G. corrected and improved the manuscript. The final manuscript was read and accepted by all contributors.

Competing interests

The authors declare no competing interests.

Additional information

Supplementary Information The online version contains supplementary material available at https://doi.org/10.1038/s41598-023-29265-w.

Correspondence and requests for materials should be addressed to L.J.B.

Reprints and permissions information is available at www.nature.com/reprints.

Publisher's note Springer Nature remains neutral with regard to jurisdictional claims in published maps and institutional affiliations.